AIP | The Journal of Chemical Physics

Structural behavior and dynamics of an anomalous fluid between attractive and repulsive walls: Templating, molding, and superdiffusion

Fabio Leoni and Giancarlo Franzese

Citation: The Journal of Chemical Physics **141**, 174501 (2014); doi: 10.1063/1.4899256
View online: http://dx.doi.org/10.1063/1.4899256
View Table of Contents: http://scitation.aip.org/content/aip/journal/jcp/141/17?ver=pdfcov
Published by the AIP Publishing

Structural behavior and dynamics of an anomalous fluid between attractive and repulsive walls: Templating, molding, and superdiffusion

Fabio Leoni[a] and Giancarlo Franzese
Departament de Fisica Fonamental, Universitat de Barcelona, Martí i Franquès 1, 08028 Barcelona, Spain

(Received 11 June 2014; accepted 13 October 2014; published online 4 November 2014)

Confinement can modify the dynamics, the thermodynamics, and the structural properties of liquid water, the prototypical anomalous liquid. By considering a generic model for anomalous liquids, suitable for describing solutions of globular proteins, colloids, or liquid metals, we study by molecular dynamics simulations the effect that an attractive wall with structure and a repulsive wall without structure have on the phases, the crystal nucleation, and the dynamics of the fluid. We find that at low temperatures the large density of the attractive wall induces a high-density, high-energy structure in the first layer ("templating" effect). In turn, the first layer induces a "molding" effect on the second layer determining a structure with reduced energy and density, closer to the average density of the system. This low-density, low-energy structure propagates further through the layers by templating effect and can involve all the existing layers at the lowest temperatures investigated. Therefore, although the high-density, high-energy structure does not self-reproduce further than the first layer, the structured wall can have a long-range influence thanks to a sequence of templating, molding, and templating effects through the layers. We find that the walls also have an influence on the dynamics of the liquid, with a stronger effect near the attractive wall. In particular, we observe that the dynamics is largely heterogeneous (i) among the layers, as a consequence of the sequence of structures caused by the walls presence, and (ii) within the same layer, due to superdiffusive liquid veins within a frozen matrix of particles near the walls at low temperature and high density. Hence, the partial freezing of the first layer does not correspond necessarily to an effective reduction of the channel's section in terms of transport properties, as suggested by other authors. © *2014 AIP Publishing LLC*. [http://dx.doi.org/10.1063/1.4899256]

I. INTRODUCTION

The study of the properties of liquids confined at the nanometer scale is a topic of high interest for its technological, experimental, and theoretical implications.[1–23] Furthermore, confinement plays an important role in hydrated biological systems and organic liquids.[24–27] Structural, thermodynamical, and dynamical properties of a liquid can change near an interface.[28] When the surface-to-volume ratio is large, at least along one direction as for the slit pore geometry, the effect of the confining surfaces has to be taken into account. Experiments and simulations on nanoconfined fluids show that molecules arrange in layers parallel to the surface.[9,29–31] The effect becomes stronger for decreasing temperature or increasing density, until the fluid eventually solidifies. The nature of the solid, as an amorphous or a crystal, can depend on the interparticle potential and the confinement conditions.[32–35] In different cases, the role of the interfaces can result in complex behaviors, e.g., a persisting fluid mono-layer around a spherical impurity while the rest of the system is in a polycrystal or glassy state,[36] a possible persisting amorphous water mono-layer adjacent to the hydrophilic disordered inner surface of a pore,[37] an induced phase transitions associated with the change in the number of layers as a function of walls separation,[31,38] or a change in the universality class from three-dimensional to two-dimensional as a function of the number of layers[39] or the size of a monolayer.[40] In a recent experiment,[41] Kaya and co-workers found that a thin-film water on a $BaF_2(111)$ surface remains in a high density liquid form for temperatures ranging from ambient (300 K) to supercooled (259 K). The result is unexpected because, based on thermodynamics arguments,[42,43] Kaya and co-workers[41] would expect that the templating effect of $BaF_2(111)$ on the structure of the water film should promote the tetrahedral structure of the low-density liquid. Moreover, the presence of an interface can promote the heterogeneous nucleation of the crystal. However, recent experiments and simulations based on crystallographic analysis of liquids on crystals,[44] or on colloidal self-assembly,[45] show that existing theories need to be revised in these cases. Confined fluids, under suitable conditions of density and temperature, can spontaneously develop patterns, e.g., stripes, and different mesophases or more complex structures.[46,47] The confinement also affects the dynamics of the liquid. It has been found that near an interface there is a reduction of the local diffusivity of the liquid.[48]

Computer simulations can help in interpreting the experimental results for nanoconfined fluids that are difficult to understand.[41,49–52] Different numerical approaches based on first principles simulations can give detailed information, but are limited by their high computational cost. Classical

[a]Present address: School of Mechanical Engineering, Tel-Aviv University, Tel-Aviv 69978, Israel.

molecular dynamics (MD) of empirical fluid models employ parameters tested for the bulk case[53,54] that not necessarily hold in confinement. The difficulty to adopt these bulk fluid models for the case of confinement leads to a variety of simulation results concerning the aggregation state of the fluid near the surfaces that in principle are model-dependent. It is, therefore, useful to develop coarse-grained models that allow for analytic calculations[55–65] and more efficient simulations,[66] like isotropic pairwise core-softened potentials. These category of potentials can allow us to better understand common features of fluids under confinement and the basic mechanisms of complex phenomena emerging in these systems, like formation of patterns and mesophases. This has been confirmed in a recent work[67] in which the authors claim that the origin of quasi-crystals could be understood in the context of a coarse-grained model by the competing effect of the hard and soft core radius of interacting particles.

Here, we perform MD simulations to study a system of confined particles interacting through the continuous shouldered well potential (CSW), an isotropic pairwise core-softened potential with a repulsive shoulder and an attractive well,[68–70] described in Sec. II A. The CSW model is suitable for studying globular proteins in solution,[71] and is possibly relevant for biological and technological applications,[72,73] colloids,[74–76] liquid metals.[77,78] In particular, the CSW reproduces density, diffusion, and structure anomalies following the water hierarchy and displays a liquid-gas and a liquid-liquid phase transition, both ending in critical points.[69,70]

The slit pore confinement is given by an attractive wall with structure and a parallel, repulsive wall with no structure, as described in Sec. II B. We calculate structural and dynamical properties in Sec. III, from which we find that the system organizes forming layers parallel to the walls with coexisting homogeneous fluid, heterogeneous fluid, and solid phases, depending on T and the average density ρ of the system. We observe that the influence of the walls can extend to the entire system, that in our case consists of up to 11 layers, through a sequence of "templating" and "molding" effects of the attractive wall. A particularly intriguing result is the discovery of "liquid veins" at low T and high ρ in the first layers. These veins are superdiffusive inducing a largely heterogeneous dynamics in the system and having a relevant effect over the transport properties of the confined fluid under extreme conditions. In Sec. IV, we present our conclusions.

II. METHODS

A. The model

We consider a system of identical particles interacting by means of the CSW potential confined between two parallel walls. The CSW potential (inset Fig. 1) is defined as[68]

$$U(r) \equiv \frac{U_R}{1+\exp(\Delta(r-R_R)/a)} - U_A \exp\left[-\frac{(r-R_A)^2}{2\delta_A^2}\right] + \left(\frac{a}{r}\right)^{24}, \quad (1)$$

where a is the diameter of the particles, R_A and R_R are the distance of the attractive minimum and the repulsive radius, respectively, U_A and U_R are the energies of the attractive well and the repulsive shoulder, respectively, δ_A^2 is the variance of the Gaussian centered in R_A, and Δ is the parameter which controls the slope between the shoulder and the well at R_R. The parameters employed are the same as in Refs. 68–70: $U_R/U_A = 2$, $R_R^* = R_R/a = 1.6$, $R_A^* = R_A/a = 2$, $(\delta_A^*)^2 = (\delta_A/a)^2 = 0.1$. In order to reduce the computational cost, we impose a cutoff for the potential at a distance $r_c/a = 3$. In the present simulations, we use $\Delta = 15$ that allows to better emphasize the anomalies in density, diffusion, and structure.[68–70]

B. Theoretical and simulation details

We consider a NVT ensemble composed of $N = 1024$ particles at fixed temperature T and volume V. The temperature of the thermal bath T is kept constant by rescaling the velocity of the particles at each time step by a factor $(T/\mathcal{T})^{1/2}$, where $\mathcal{T}$ is the instantaneous kinetic temperature (Allen thermostat).[79] Pressure, temperature, density, diffusion constant, and time are all expressed in internal units: $P^* \equiv Pa^3/U_A$, $T^* \equiv k_BT/U_A$, $\rho^* \equiv \rho a^3$, $D^* \equiv D(m/a^2U_A)^{1/2}$, and $t^* \equiv (a^2m/U_A)^{1/2}$, respectively, with a unit of distance. For sake of simplicity, in the following we will drop all the * denoting internal units. The equations of motion are integrated by means of the velocity Verlet method,[79] using the time-step $dt = 0.0032$ (that corresponds to $\sim 1.7 \times 10^{-12}$ s for water-like molecules and to $\sim 2.1 \times 10^{-12}$ s for argon-like atoms[70]). We performed the same check as in Ref. 70 in order to verify that the value used for dt is small enough to satisfy the energy conservation of the system.

The confining parallel walls are placed along the z axis at a separation distance L_z. The attractive wall is composed of a triangular lattice of CSW particles quenched with the position of the centers placed at $z_{\text{attr}} = 0$. The lattice constant is $d = a$. The repulsive wall has no structure and is obtained by imposing the repulsive potential $U_{\text{rep}}(z) \equiv [\sigma/(L_z - z)]^9$ where z is the position of the fluid particle.[80] In the following, we consider the parameter $\sigma = a$. We adopt periodic boundary conditions in the x and y directions. In order to compute the effective density ρ_{eff}, we compute the effective volume V_{eff} accessible to particles $V_{\text{eff}} \equiv L_z^{\text{eff}}A$, where $A \equiv L_xL_y$ is the section of the simulation box and L_z^{eff} is the effective distance between the plates. By considering the quenched particles forming the attractive wall and the repulsive strength of the potential of the repulsive wall, we obtain $L_z^{\text{eff}} \simeq L_z - a/2 - (1/T)^{1/9}$.[80] The effective density is $\rho_{\text{eff}} \equiv \rho_{\text{eff}}(\rho, T) \equiv \rho \cdot (L_z/L_z^{\text{eff}})$.

To explore different densities for the confined system in the NVT ensemble, we change L_x and L_y. We keep L_z and N constant to exclude finite-size effects when we compare results for different densities. For each density, we equilibrate the system by annealing from $T = 4$. For each temperature, the system is equilibrated during 10^6 time steps. We observe equilibrium after 10^4 time steps for the range of ρ and T considered here. All our results are averaged over 10 independent samples. In order to check the stability of the system, we verify that the energy and the pressure are equilibrated. The

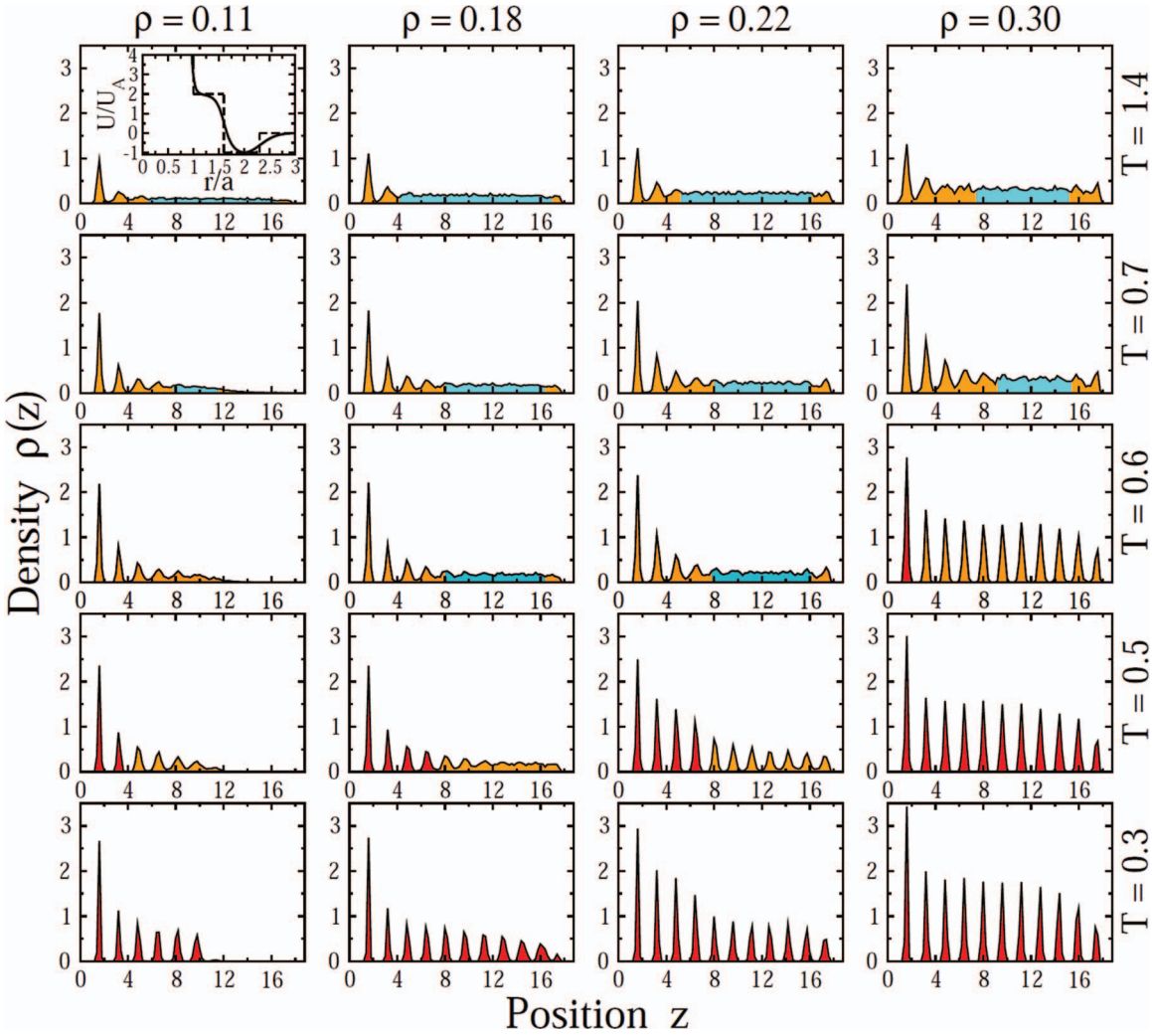

FIG. 1. Density profile $\rho(z)$ for CSW particles at densities $\rho = 0.11, 0.18, 0.22, 0.30$ and temperatures $T = 1.4, 0.7, 0.6, 0.5, 0.3$ confined in a slit pore with an attractive, structured, wall at position $z_{attr} = 0$ and a parallel, repulsive wall, without structure, at position $z_{rep} = L_z$ along the z axis. Based on the analysis in Secs. III B–III E, we find that, depending on T and ρ the system separates into different phases: a homogeneous fluid in the central region of the slit pore (for those z coordinates corresponding to the regions in cyan), a heterogeneous fluid near the walls (in orange) and solid phase, made of crystals or stripes, that forms near the attractive wall at low T and ρ and propagates toward the repulsive wall at higher ρ (in red). Inset: the CSW interparticle potential.

pressure of the confined fluid is calculated as indicated in Sec. A of the supplementary material.[81]

III. RESULTS AND DISCUSSION

A. Density profile and aggregation state

As pointed out in the Introduction (Sec. I), the confinement can modify the structure of a fluid resulting in an inhomogeneous density profile. In a slit pore geometry, near the confining walls, particles form layers parallel to the walls as the temperature is decreased or the density is increased, as shown by our calculations for the density profile $\rho(z)$ (Fig. 1).

At high $T = 1.4$ and low $\rho = 0.11$, we find only one well defined layer near the attractive wall and no layering near the repulsive wall, while the whole system is in the fluid state. By decreasing T and increasing ρ, the number of layers increases up to 11. Furthermore, for $\rho \geq 0.18$, the layers also appear near the repulsive wall. However, we observe that away from the walls the system is a homogeneous fluid state for intermediate density ($\rho = 0.18$ and 0.22) for $T = 0.6$ and for any of the considered ρ for $T > 0.6$.

Nonetheless, the walls can affect the density profile over the entire system, in our case made up to 11 layers, at $T \leq 0.6$. In particular, we observe a change in the system density and aggregation state.

To establish the aggregation state for each layer, we compute, layer by layer, a series of structural and dynamical quantities described in Secs. III B–III E, that, all together, allow us to identify the presence and coexistence of a homogeneous fluid, a heterogeneous fluid, and a solid made of polycrystals or stripes phases.

B. Radial distribution function and spatial configuration analysis

The in-layer radial distribution function $g_{\parallel}^{n}(r_{\parallel})$ for the nth layer (with $n = 1, 2, \ldots, 11$) is computed as

$$g_{\parallel}^{n}(r_{\parallel}) \equiv \frac{1}{(\rho^n)^2 A \delta z} \sum_{i \neq j} \delta(r_{\parallel} - (r_{ij})_{\parallel}) \left[\Theta\left(\frac{\delta z}{2} - |z_i - z^n|\right) \times \Theta\left(\frac{\delta z}{2} - |z_j - z^n|\right) \right], \quad (2)$$

where ρ^n and z^n are the density of particles and the z-coordinate of the layer n, respectively. The product of Heaviside step functions, Θ, select pairs of particles i and j that lie in the layer n of width δz, centered around z^n, and the Kronecker δ-function selects two particles at distance $r_{||} \equiv (x^2 + y^2)^{1/2}$ in the layer. The $g_{\|}^n(r_{\|})$ is proportional to the probability of finding a particle in the layer n at a distance $r_{\|}$ from a randomly chosen particle of the same layer n. The definition of the layer n in which lies a particle i is established according to the value of the z-coordinate of the particle i, following the separation in layers of thickness $\approx\delta_z$ described in Sec. III A: for the first layer $0 < z_i^{n=1} < (3/2)\delta_z$, with $\delta_z = R_R$, and $(j - 1/2)\delta_z < z_i^{n=j>1} < (j + 1/2)\delta_z$ for the others.

1. Low density

At low density ($\rho = 0.11$, Fig. 2), we observe that the system is in a fluid state for high temperature ($T = 1.4$) in any layer. The $g_{\|}^n(r_{\|})$ of the layer $n = 1$ shows a first peak around the shoulder radius ($r_{\|} \simeq 1.6$) and a second peak around the attractive well radius ($r_{\|} \simeq 2$), while for the other layers only the second peak is present. We interpret this difference between the first and the other layers as the consequence of a "templating" effect of the attractive wall. This effect due to the attraction to the wall is so strong to force particles in the first layer to be at their repulsive distance. As we discuss in the following, the effect is stronger at lower T.

At $T = 0.7$, the system shows the same behavior observed for higher temperatures, except that the layer near the attractive wall develops patterns. This behavior is reminiscent of what has been observed in monolayers with an interparticle potential composed by a hard core and a soft repulsive shoulder.[46]

At $T = 0.6$, the layer near the attractive wall is still showing patterns, while the layer $n = 2$ is forming crystal patches. This is evident from the analysis of the $g_{\|}^{n=2}$ that goes to zero for $r_{\|} \simeq 2.75$ and 4.75 at $T = 0.6$, consistent with an incipient triangular crystal with lattice step given by the interaction potential attractive distance $R_A = 2$. The other layers are in a fluid state.

At $T = 0.5$, the first layer is forming a hexagonal crystal. Although the hexagonal crystal in $n = 1$ does not overlap exactly with the triangular wall structure, the comparison of the $g_{\|}^{n=1}$ and $g_{\|}^{n=0}$ of the wall shows a strong correlation between the two structures, suggesting a "templating" effect. The high-energy cost of the resulting hexagonal lattice forming in the

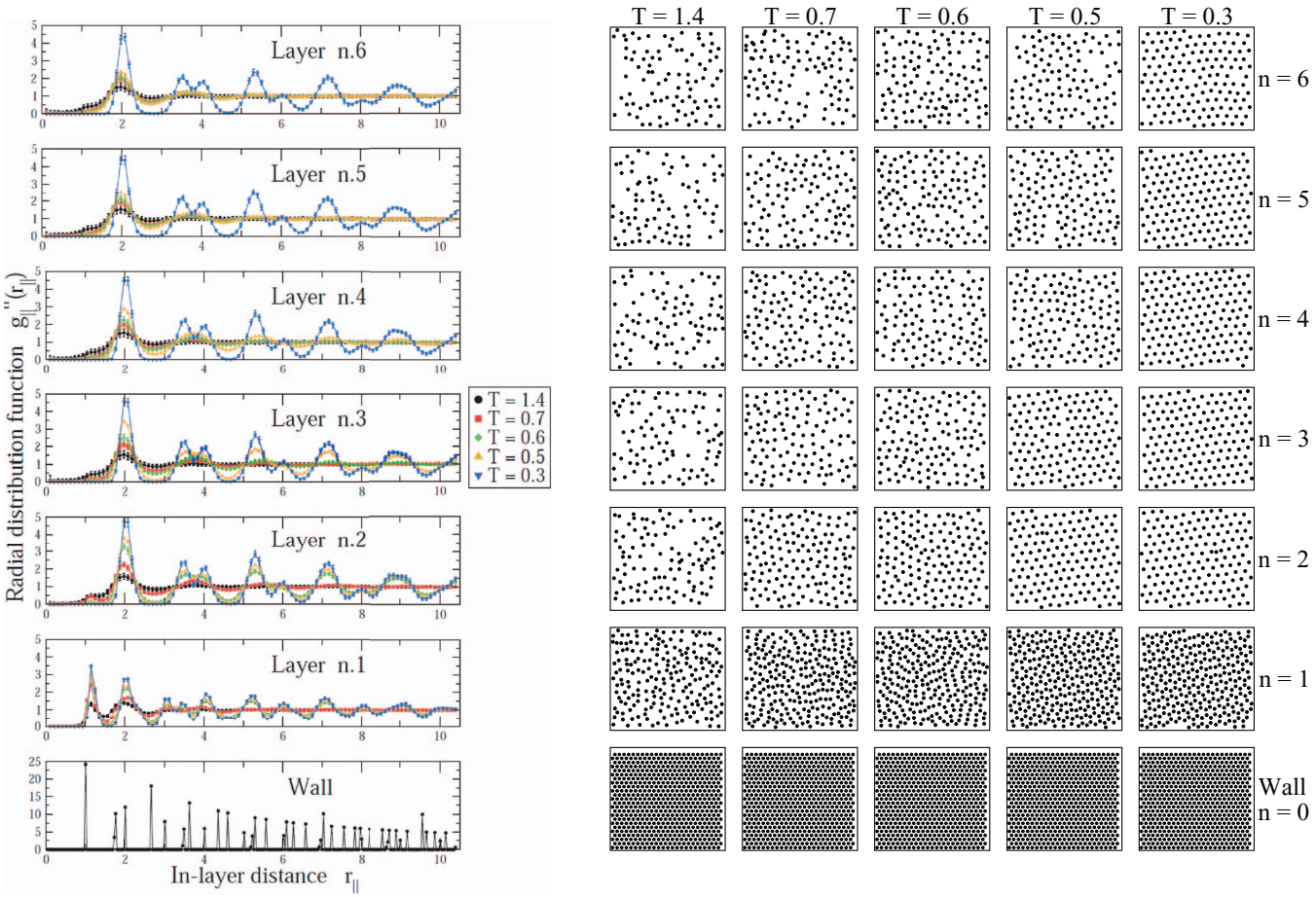

FIG. 2. Left: In-layer radial distribution function $g_{\|}^n(r_{\|})$ for $\rho = 0.11$ for (from bottom to top) the wall and the particles in the first six layers, for temperatures $T = 1.4$, 0.7, 0.6, 0.5, 0.3 (with colors as indicated in the legend) and effective densities (see Sec. II B) $\rho_{\text{eff}} = 0.1193$, 0.1198, 0.1200, 0.1201, 0.1205, respectively. Right: Typical particle configurations, after $t = 10^6$ MD steps, for different temperatures (top-most labels) and layers (right-most labels). The snapshots are projections on the xy-plane of the coordinates of particles in each layer.

layer $n = 1$ is compensated by the large number of attractive interactions between the particles at $n = 1$ and those of the wall ($n = 0$) from one hand, and between the particles themselves at $n = 1$ from the other hand. This free energy minimization process is analyzed in Sec. C of the supplementary material[81] in the discreet potential approximation.

The triangular structure that was incipient for $n = 2$ at high T, for $T = 0.5$ is well defined for $n = 2$ and $n = 3$, with defects in the layer $n = 3$. This triangular structure is the dual lattice of the $n = 1$ hexagonal layer and its formation is the consequence of a "molding" effect of the layer $n = 1$ onto the layer $n = 2$. Note that while the wall ($n = 0$) layer has a templating effect on the $n = 1$ layer, the $n = 1$ layer has a molding effect on the $n = 2$ layer. The difference between the two cases is due to the first layer density smaller than the wall density. The smaller density does not allow to compensate the high energy cost of the propagation of the hexagonal crystal to the layer $n = 2$. On the other hand, the triangular crystal of the $n = 2$ layer is energetically favorable, because the particles are all at the attractive distance, and at this T the triangular structure can propagate to the $n = 3$ by "templating." The layer $n = 4$ is made of a few triangular crystallites immersed in the fluid, while the other layers are in the fluid state.

At $T = 0.3$, both the templating and the molding effect are stronger. In particular, the template of the $n = 2$ layer propagates over all the six layers that are formed at this density and temperature.

2. Intermediate density

At intermediate density ($\rho = 0.22$, Fig. 3), for $T = 1.4$ and $T = 0.7$ we observe the same qualitative behavior as for the low density case. For $T = 0.6$, the layer $n = 1$ has less tendency to form patterns respect to the low-density case, and the layer $n = 2$ has less tendency to crystallize. Therefore, the confined system is more fluid at this density than at lower density. We understand this result as a consequence of the larger number of layers in the slit pore for higher density and the increased probability for each particle to interact with another that is outside the wall attractive range.

At $T = 0.5$, the first layer partially crystallizes in the hexagonal lattice and partially in the triangular structure following the template of the wall. Therefore, the templating effect is now stronger than the corresponding case at lower density. The hexagonal crystal shows now a preferred direction of symmetry. This direction propagates to the layer $n = 2$, where

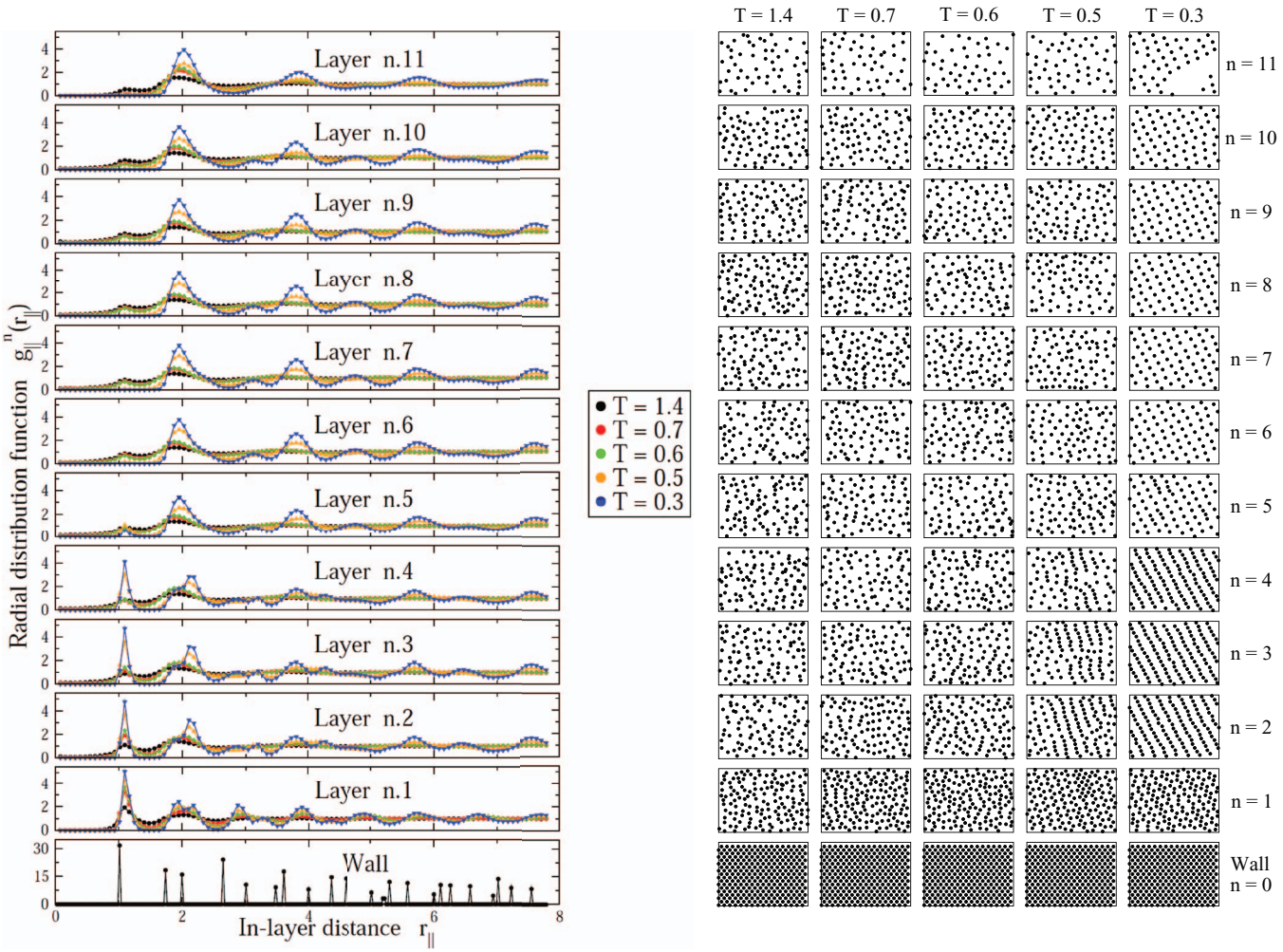

FIG. 3. As Fig. 2, but for $\rho = 0.22$. The effective densities (see Sec. II B) that correspond to $\rho = 0.22$ and temperatures $T = 1.4$, 0.7, 0.6, 0.5, 0.3 are $\rho_{\text{eff}} = 0.2386$, 0.2397, 0.2399, 0.2402, 0.2411, respectively.

we observe stripes along the preferred direction. The stripes propagate up to $n = 4$ layer, while the other layers are in a fluid state. The peak of $g_{\parallel}^{n}(r_{\parallel})$ at $r_{\parallel} \simeq 2.1$ (that corresponds to the average second nearest neighbor distance) is a signature of the stripe phase formation.

At $T = 0.3$, the preferred direction in the deformation of the hexagonal crystal for $n = 1$ is more evident and we observe a clear stripe phase for the layers from $n = 2$ to $n = 4$, with a peak of $g_{\parallel}^{n}(r_{\parallel})$ at $r_{\parallel} \simeq 2.1$ more pronounced than the case at $T = 0.5$. The other layers form a square crystal at the attractive distance.

3. High density

At high density ($\rho = 0.30$, Fig. 4), for $T = 1.4$ we observe the same qualitative behavior as for the lower density cases. At $T = 0.7$, we find that the only difference with the lower density case is that the layer $n = 1$ is forming triangular crystallites following the template of the wall.

At $T = 0.6$, the layer $n = 1$ has a different and incipient crystal structure (Kagome lattice) with defects that is better defined at lower T. This is evident from the analysis of the $g_{\parallel}^{n=1}$ that goes to zero for $r_{\parallel} \simeq 1.6$ and 2.75 at $T = 0.6$. The layer $n = 2$ shows patterns very close to the stripe configuration. The corresponding $g_{\parallel}^{n=2}$ goes to zero for $r_{\parallel} \simeq 1.5$ and shows a peak for $r_{\parallel} \simeq 2.1$. These characteristics of the $g_{\parallel}^{n}$ are typical of a stripe phase. The layer $n = 3$ and $n = 4$ still show patterns close to the stripe phase, but in a less pronounced way. From the layer $n = 5$ to the $n = 10$ the pattern is vanishing. The layer $n = 11$ is showing an incipient triangular crystal with lattice step given by the interaction potential attractive distance $R_A = 2$. This is evident from the analysis of the $g_{\parallel}^{n=11}$ that approaches zero for $r_{\parallel} \simeq 2.75$ and 4.75 at $T = 0.6$.

At $T = 0.5$, the layer $n = 1$ is forming a Kagome crystal with defects. The layers from $n = 2$ to $n = 10$ show a stripe phase and the layer $n = 11$ is forming a triangular crystal with defects.

At $T = 0.3$, the Kagome crystal of layer $n = 1$ has no defects. The layers from $n = 2$ to $n = 10$ are in a stripe phase and the layer $n = 11$ is forming a well defined triangular crystal.

In Sec. B of the supplementary material,[81] we compare the templating effect on the first layer for different densities. In particular, we observe how the crystallization of the

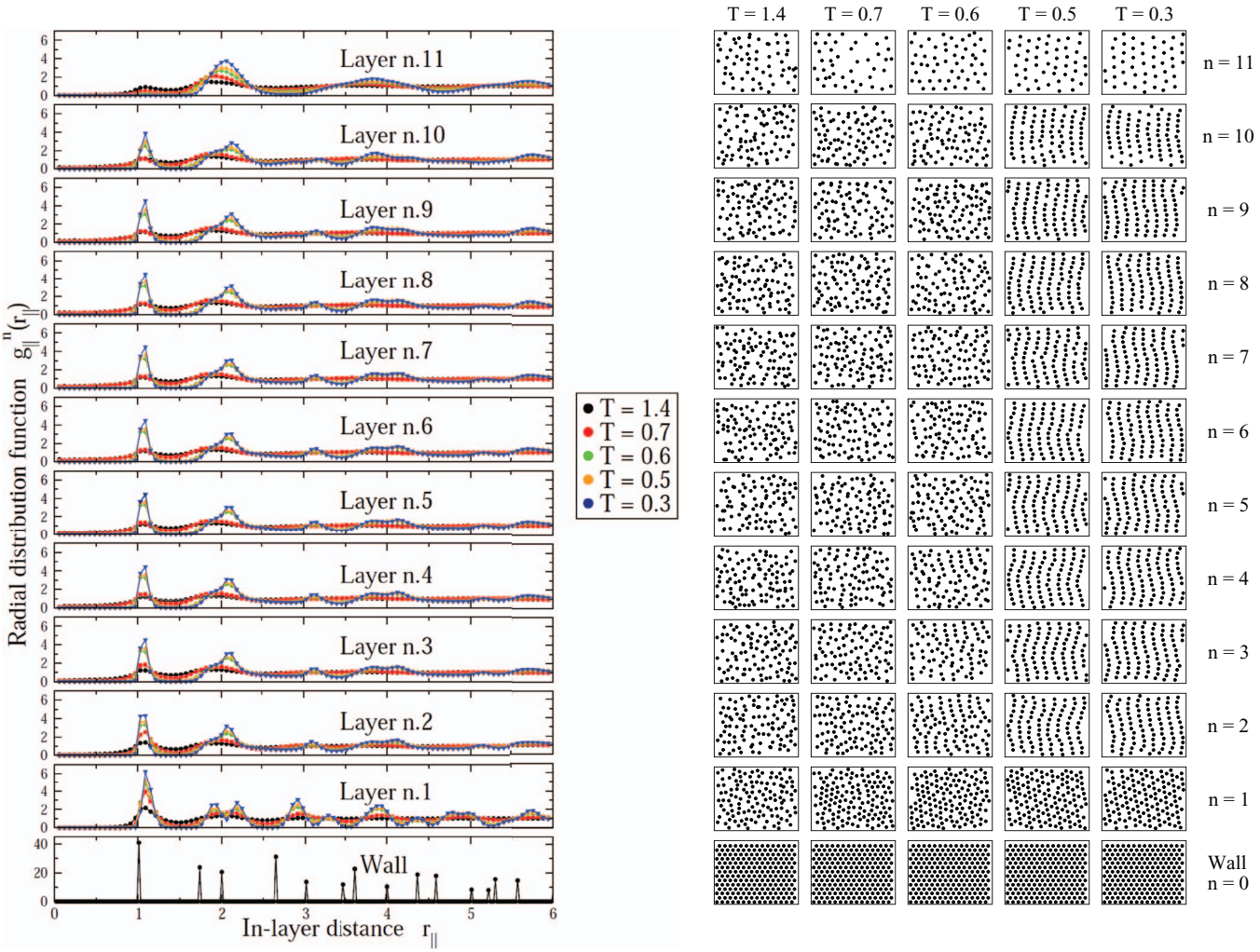

FIG. 4. As Fig. 2, but for $\rho = 0.30$. The effective densities (see Sec. II B) that correspond to $\rho = 0.30$ and temperatures $T = 1.4$, 0.7, 0.6, 0.5, 0.3 are $\rho_{\text{eff}} = 0.3254$, 0.3268, 0.3272, 0.3276, 0.3288, respectively.

first layer changes progressively from the hexagonal lattice to the square and, next, to the Kagome lattice by increasing the density of the system, as consequence of the interplay of the template of the attractive wall and the interparticle potential.

We also show, in Sec. III E, by performing the Voronoi structural analysis of the layers near the attractive wall, that the first layer at low T is a frustrated polycrystal and that the increase of density induces an increase of frustration in the first and the other solid layers. The system cannot reach easily the global minimum of the free energy landscape, corresponding to the crystal configuration, but is trapped in local minima due to the slowing down of the dynamics (see Secs. III C and III D) and the templating effect of the attractive wall. In particular, the mismatch of the wall structure with the bulk crystal structure induces a frustrating effect that is more evident near the wall (in layers $n = 1$ and $n = 2$) for increasing density.

Furthermore, in Sec. C of the supplementary material,[81] we show that, if a layer has a triangular structure, as the stable configuration of layers $n = 2, \ldots, 6$ at low density (Fig. 2), then for sufficiently high density the system will prefer to form stripes within the same layers.

C. Mean square displacement (MSD) analysis

In order to characterize space-dependent diffusion properties of our system, we compute the MSD associated to each layer of the slit pore (Fig. 5). We observe that, except for low T, a particle can travel across layers with different aggregation state. Hence, we calculate the MSD only for those particles that remain in a layer over the entire time interval under consideration and we average over all possible time intervals. Therefore, the MSD associated to each layer n is defined as

$$\langle(\Delta r^n_{||}(\tau))^2\rangle \equiv \langle(r^n_{||}(t - t_0) - r^n_{||}(t_0))^2\rangle, \tag{3}$$

where $\tau \equiv t - t_0$ is the time spent in the layer n by a particle that enters the layer at time t_0.

The diffusion coefficient $D_{||}$ in the direction parallel to the walls is by definition a constant given by $D_{||} \equiv \lim_{\tau\to\infty}\langle(\Delta r^n_{||}(\tau))^2\rangle/(4\tau^\alpha)$ where α is the diffusion

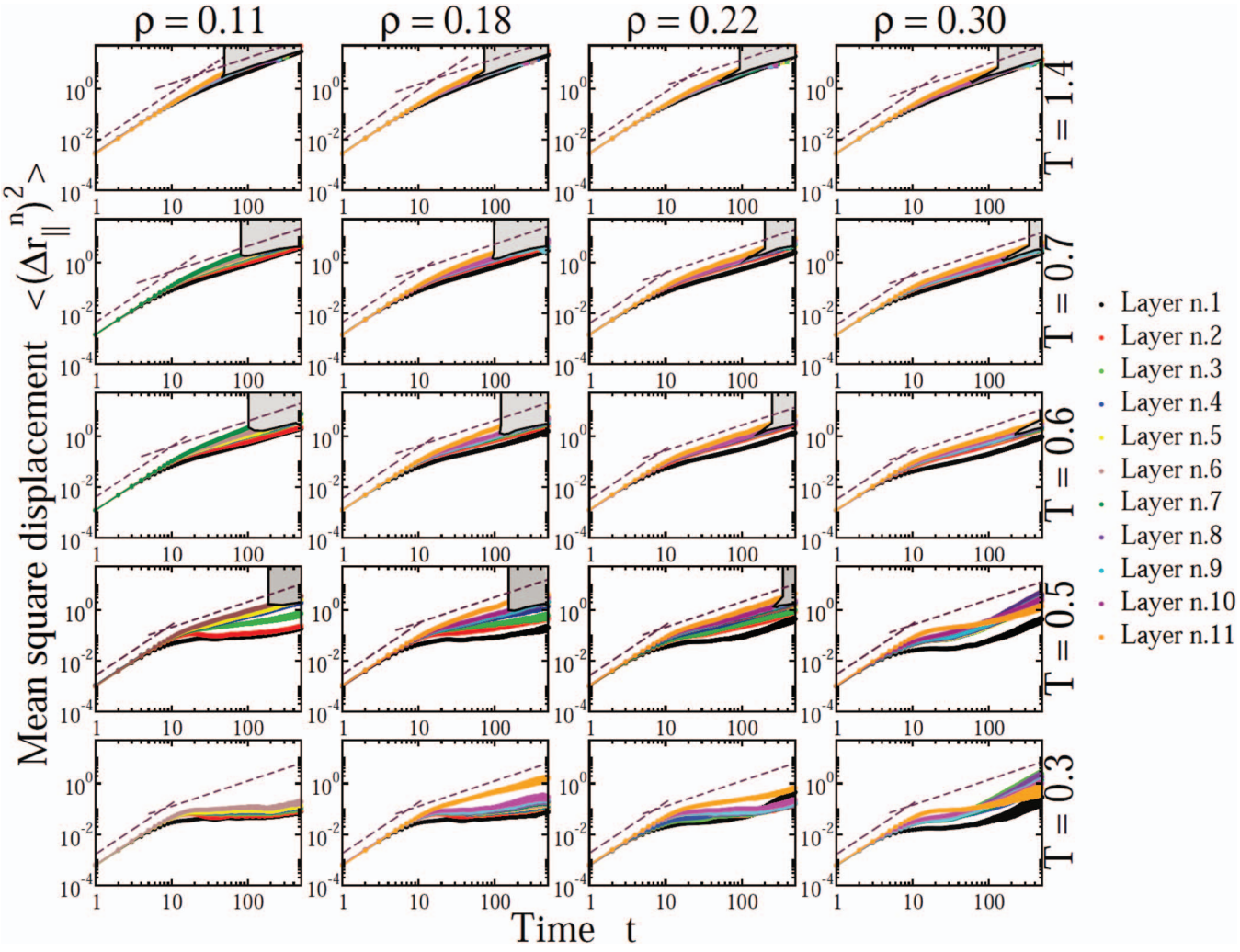

FIG. 5. In-layer mean square displacement (MSD) as a function of time, t, for fluid densities $\rho = 0.11, 0.18, 0.22, 0.30$ (top-most labels) and temperatures $T = 1.4, 0.7, 0.6, 0.5, 0.3$ (right-most labels) for CSW particles in the slit-pore confinement, with layer $n = 1$ (in black) adjacent to the attractive wall and layer $n = 11$ (in orange) next to the repulsive wall. Intermediate layers have different colors, as indicated in the legend. Dashed lines represent the ballistic and diffusive regimes at early and long times, respectively. The gray regions give an indication of the time interval over which the MSD is not well defined, as discussed in Sec. III D. At low T and high ρ, we observe a large heterogeneity for the dynamics of different layers.

exponent that characterizes the dynamics of the system. For an arrested system, as in a solid state where particles can only vibrate around theirs equilibrium positions, is $\alpha = 0$. For a subdiffusive system, corresponding in general to particles diffusing in complex structures (with non-trivial microscopic disorder), is $0 < \alpha < 1$. For a diffusive system in a normal fluid state is $\alpha = 1$. For $\alpha > 1$ the system is superdiffusive.

Our analysis shows that the in-layer MSD has always a ballistic regime, $\langle(\Delta r_{\parallel}^{n}(\tau))^2\rangle \sim \tau^2$, for $t \leq 10$. The corresponding mean displacement is approximately half particle diameter at high T and low ρ, weakly decreasing for increasing ρ and decreasing T, as expected for the decrease of the particles mean free path (Fig. 5).

For $T \geq 1.4$, all the layers reach the diffusive ($\alpha = 1$) behavior for long times. By decreasing the temperature the behavior of the layers becomes more heterogeneous. In particular, we observe that at $T \leq 0.7$ the layer $n = 1$ near to the attractive wall slows down in a sensible way with respect to the other layers and becomes arrested for $T \leq 0.5$. At these temperatures the other layers, including the $n = 11$ near the repulsive wall, are diffusive at low densities.

However, at $\rho = 0.30$ and $T = 0.5$ the MSD for all the layers develop the plateau that is typical of glassy dynamics. This behavior is reminiscent of the caging effect in glasses where the plateau in the MSD is followed by a diffusive regime. Here, instead, at $T = 0.5$ and $\rho = 0.30$ we observe that for all the layers, but the one near the repulsive wall ($n = 11$), after the plateau, the dynamics enters in a superdiffusive regime with $1 < \alpha < 2$. This effect is related to the presence of defects and of a nonuniform stress field, as discussed in Sec. III F.

For $T = 0.3$, we observe that all the layers are arrested at $\rho = 0.11$. At this low density the slit pore is only partially filled (Fig. 1). At $T = 0.3$ and $\rho = 0.18$ and $\rho = 0.22$ also the layer $n = 11$ near the repulsive wall is present and it is characterized by a larger MSD with respect to the other layers and by a diffusive regime at long times. The other layers have an arrested dynamics. At $T = 0.3$ and $\rho = 0.30$, all the layers from $n = 1$ to $n = 10$ have a superdiffusive regime at long times, while the layer $n = 11$ reaches the diffusive log-time regime. However, its MSD is smaller than that of the other layer for very long times ($t \geq 100$).

D. Survival probability (SP) function analysis

As the time proceeds, the average in Eq. (3) for the MSD is performed on a decreasing number of particles because some of them can leave the layer. *A priori* this reduction of the statistics is not homogeneous in the sense that the particles that leave the layer are, in general, those with larger velocity, inducing a bias in the MSD calculation. Therefore, for $T \geq 0.5$, at low enough ρ, and for the most diffusive layers there is a time, $\tau_{\max}$, after which the in-layer MSD is not well defined (gray region in Fig. 5).

To estimate $\tau_{\max}$ as function of T and ρ for different layers, we analyse the population relaxation of particles in each layer. In particular, we compute the in-layer survival probability (SP) function, $S_n(\tau)$, which is the probability that a given particle stay in the layer n for a time interval τ. We define the SP as

$$S_n(\tau) \equiv \left\langle \frac{N_n(t, t+\tau)}{N_n(t)} \right\rangle, \tag{4}$$

where $N_n(t)$ is the number of particles in the layer n at time t and $N_n(t, t + \tau)$ is the number of particles that do not leave the layer n during the time interval $[t, t + \tau]$. The SP give an indication of the time interval $\tau_{\max}$ over which the MSD is well defined. We observe that $S_n(\tau)$ has an exponential decay in our simulations for all layers (Fig. 6).

We, therefore, define $\tau_{\max}^{n}$ as the characteristic decay time $S_n(\tau) \sim e^{-\tau/\tau_{\max}^{n}}$, associated to the layer n. This choice is consistent with the observation that the MSD (Fig. 5) is well defined when $S_n(\tau) \geq 1/e$.

We observe that for $T \geq 0.6$ and all the densities and for $T = 0.5$ and $\rho \leq 0.22$, the SP decay is slower for the layer $n = 1$ near the attractive wall and is faster for the layers away from the two walls. When the layer $n = 11$ near the repulsive wall is present, we observe that it has a decay in SP slower than those layers that are farther away from the wall. At $T = 0.3$ for all densities, and at $T = 0.5$ for $\rho = 0.30$, there is no decay in SP, consistent with the crystallization of the layers.

Hence, $\tau_{\max}$ is non-monotonic as a function of the z-coordinate (Fig. 7) for the majority of densities and temperatures investigated here and is larger for the layers that are more structured (Fig. 1). Therefore, both walls facilitate the slowing down of the dynamics of the fluid, although the effect associated to the structureless and repulsive wall is weaker than the effect of the structured and attractive wall. This result is reminiscent of what has been found for water confined in both hydrophobic and hydrophilic walls.[82]

E. Voronoi structural analysis of the solid

Our MSD and SP analysis (Figs. 5–7) show that at low T and high ρ there are layers that behave as a solid. However, by looking only at the MSD and SP is not possible to establish if a solid layer is in an amorphous, crystal, or polycrystal state.[83] In order to better understand the structure of solid layers, we use the standard 2d Voronoi tessellation (useful to identify defects present in the crystal structures, as vacancies, Frenkel-like, dislocations and grain boundaries). In particular, we adopt a modified version of it that is more suitable to identify distorted crystal structures.

Following the standard Voronoi tessellation, Voronoi cells are polygons with edges that cross the middle point of the lines connecting the particles of a configuration. As a consequence, each Voronoi cell contains one and only one particle and represents the proper volume of the particle in its center. This procedure generates cells with different numbers of edges – at least three – some of which can be very short. The very short edges represent small lattice deformations that are irrelevant for the structural inspection of the configuration. Therefore, to reduce the noise in our analysis, we choose to neglect the edges whose length is less than 10% of the average length of all the edges of the polygon they belong.

With this modified Voronoi tessellation we analyze the structure of different configurations. At low density

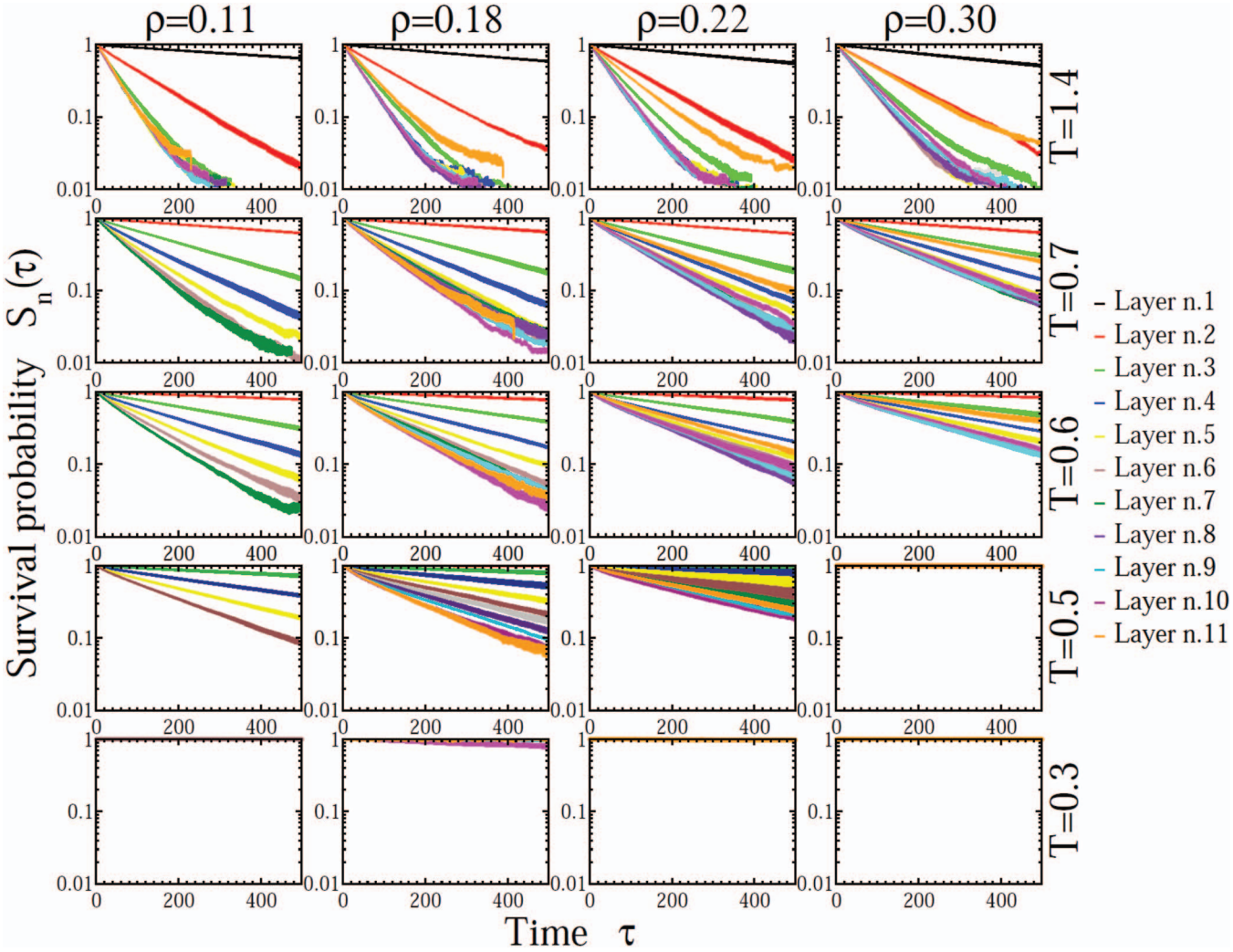

FIG. 6. The in-layer survival probability (SP), $S_n(\tau)$, as a function of the time interval τ, for $\rho = 0.11, 0.18, 0.22, 0.30$ (top-most labels) and $T = 1.4, 0.7, 0.6, 0.5, 0.3$ (right-most labels) for CSW particles in a slit pore confinement, with the layer $n = 1$ (in black) near the attractive wall and the layer $n = 11$ (in orange) near the repulsive wall. Other layers have different colors, as indicated in the legend. The layers with a faster decay of $S_n(\tau)$ are, in general, those away from the two walls of the slit pore.

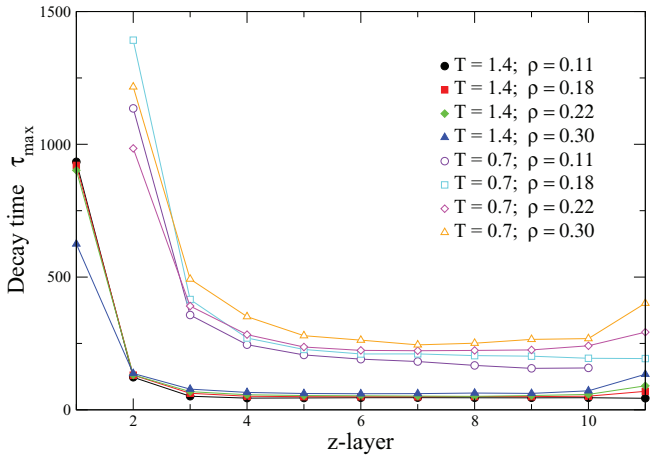

FIG. 7. Characteristic decay time τ_{max} as a function of fluid layer for density $\rho = 0.11, 0.18, 0.22, 0.30$ and temperature $T = 1.4, 0.7$. For clarity, the points for $T = 0.7$ are shifted up by 100 units.

($\rho = 0.11$) and $T = 0.3$, we observe that in all our simulations the first layer near the attractive wall is in a frustrated solid state mainly composed by a distorted hexagonal lattice (Fig. 8(a)).

By annealing these configurations, with an annealing rate of $0.025U_A^{3/2}/(k_B a m^{1/2})$, to $T = 0.0005$ we find that the first layer becomes a frustrated polycrystal (Fig. 8(b)). The polycrystal has point and line defects as grain boundaries dividing a hexagonal lattice (green triangles) from a stripe phase (cyan polygons).

For both $T = 0.3$ and $T = 0.0005$, the other layers are organized in a triangular lattice (cyan polygons). We observe defects, such as dislocations, that are not eliminated by annealing (Fig. 8 Run # 2).

At high density ($\rho = 0.30$), the first layer at $T = 0.3$ is in a polycrystal state with many defects (Fig. 9(a)). At $T = 0.0005$, we observe two principal crystal grains

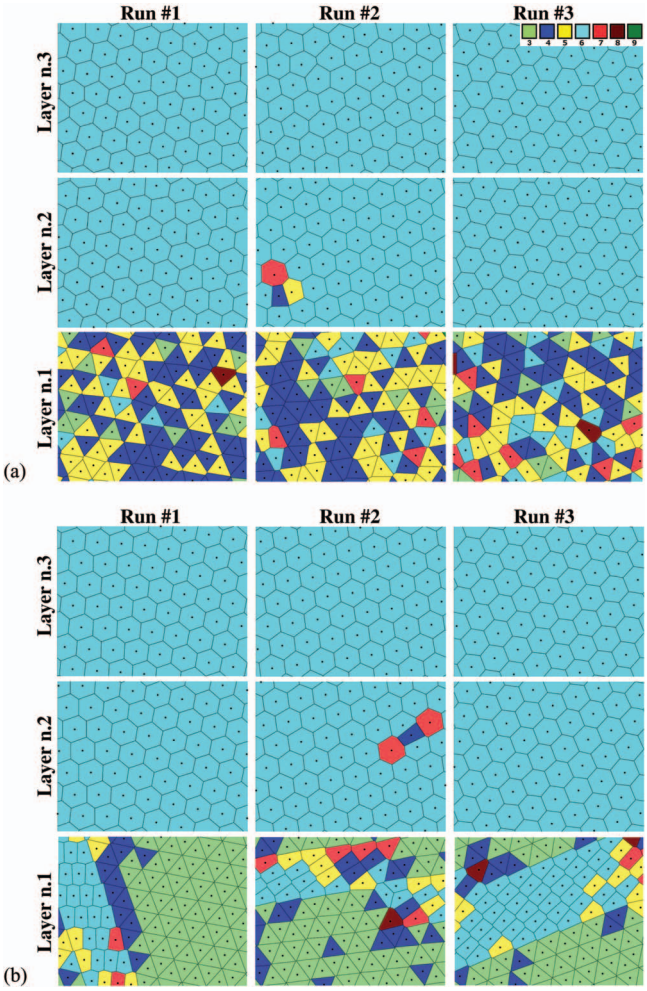

FIG. 8. Modified Voronoi tessellation (see text) for the first three layers near the attractive wall of three different realizations of our system at $\rho = 0.11$ with (a) $T = 0.3$ and (b) $T = 0.0005$. Different colors represent Voronoi cells with different number of edges: 3 (green), 4 (blue), 5 (yellow), 6 (turquoise), 7 (red), 8 (maroon). We observe polycrystal structures in the layer $n = 1$ near the attractive wall at the lowest T.

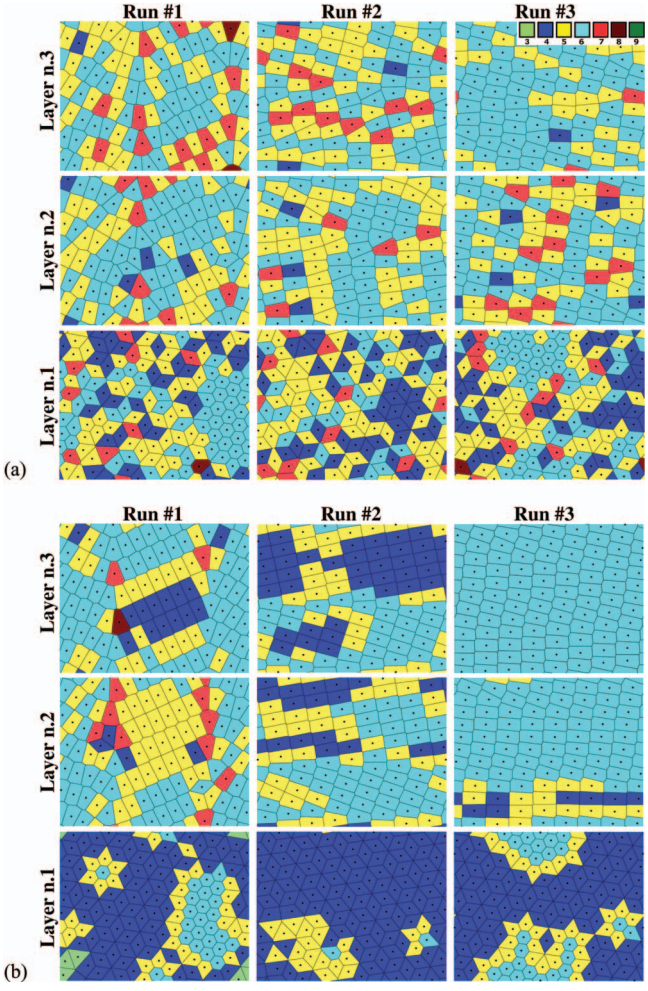

FIG. 9. As in Fig. 8, but for $\rho = 0.30$ with (a) $T = 0.3$ and (b) $T = 0.0005$. For the layer $n = 1$ the system forms a polycrystal made of a triangular lattice (cyan hexagons) and a Kagome lattice (blue rhombuses) with a number of defects that decreases with T. For layers $n = 2, 3$ it forms zigzagging stripes phases with defects.

(Fig. 9(b)): a triangular lattice (cyan hexagons) and a Kagome lattice with defects (blue rhombuses).

At $T = 0.3$, the layers $n = 2, 3$ present a zigzagging stripe structure with orientation and angles that can change from run to run. At $T = 0.0005$, the stripe structure of these layers becomes more regular.

F. Liquid veins

In Sec. III C, we have observed that for high densities and low temperatures the anomalous fluid can be superdiffusive in some layers in the long-time regime. In this section, we show how this behavior is due to the formation of "liquid veins" in such layers.

To better understand the origin of the superdiffusive dynamics, we simulate our system at $T = 0.3$ and $\rho = 0.30$ for three different realizations of the initial configuration. After equilibration, we observe that the three realizations lead to the same qualitative layer structures (Fig. 10). However, the dynamics of the three runs are different. In particular, we observe that all the particles in the first layer ($n = 1$) have the same MSD, while particles in other layers ($n = 2, 3$) can have different MSD, as in Run #1 of Fig. 11.

The differences in MSD can be understood by analyzing the trajectories of the particles in Run #1 (Fig. 12). We observe that the majority of particles in the layer $n = 2$ remain spatially localized during the entire simulation, except a few particles with mobility higher than the rest of the system. In particular, we find that the fast particles belong to two stripes and diffuse along the stripe itself, as along a liquid vein (Fig. 12(a)). We observe a similar situation for the layer $n = 3$ (Fig. 12(b)), but here all the particles are more mobile and the streams in the two veins flow in opposite directions.

In the context of the prototypical anomalous fluid–water– the formation of liquid veins during freezing is of particular interest. For example, recently, experiments and simulations showed the presence of liquid water between nanometer-sized ice crystal.[84]

More in general, in polycrystalline systems, the liquid is found along intergranular junctions, as grain boundaries, as described for the case of water in Ref. 84 and references

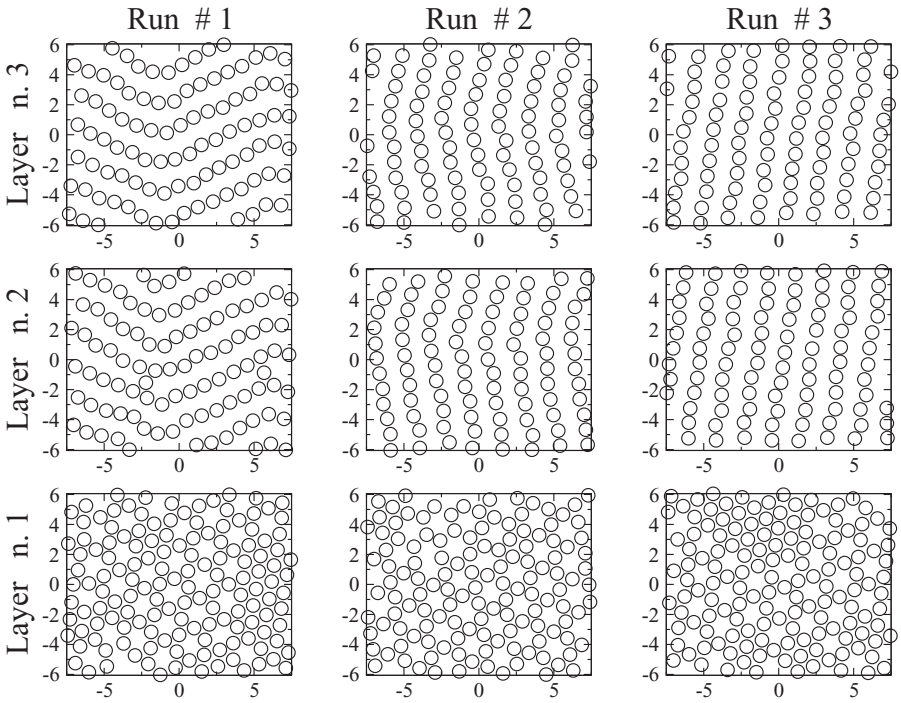

FIG. 10. Spatial configurations of CSW particles confined in slit pore for the first three layers near to the attractive wall, for three different realizations of the initial conditions at $T = 0.3$ and $\rho = 0.30$. As in Fig. 4, in each run the layer $n = 1$ forms a Kagome crystal and the others are in a stripe phase. The snapshots are projections on the xy-plane of the particles coordinates in a layer and particles have the size of their hard core.

therein. Residual stress in these polycrystal structures can be localized along intergranular junctions, and can result in an effective force that acts on fluid particles present in these junctions.

In our system, as well as in glasses, the residual stress is a consequence of the fact that when the fluid solidifies the minimization process of the free energy takes place locally, instead of globally. In glass forming liquids, this effect is caused by a fast cooling, while in our system it is due to the layering of the fluid as a consequence of the confinement. Further analysis, that goes beyond the goals of the present work, is necessary to understand the effect of the vicinity of the attractive wall

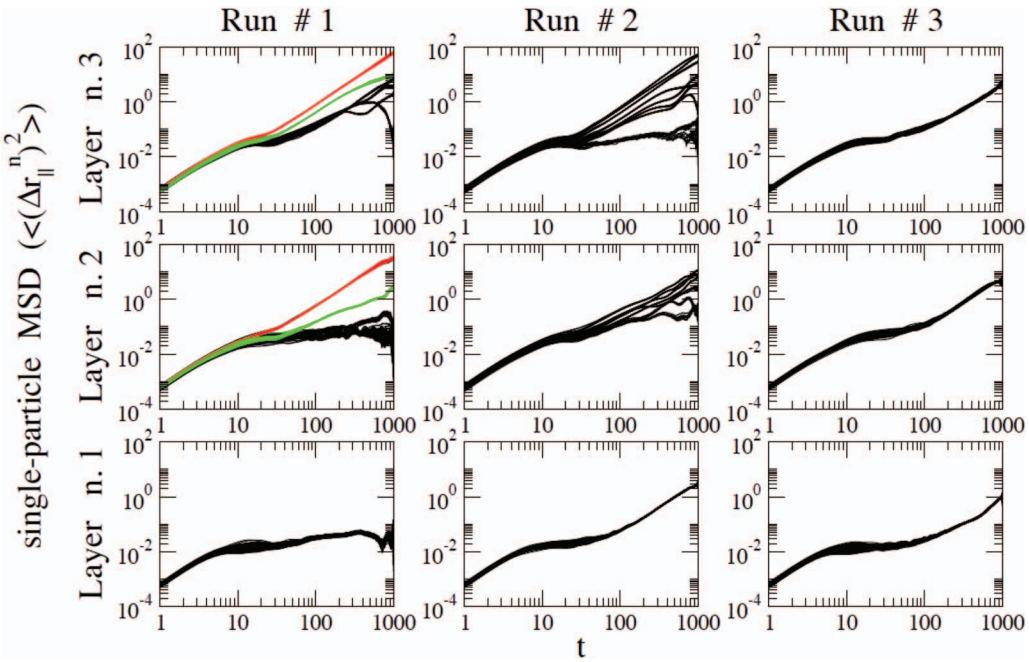

FIG. 11. Single-particle MSD for layers and runs as in Fig. 10. For Run #1, we observe a homogeneous dynamics among the particles within the layer $n = 1$, but a heterogeneous dynamics for $n = 2$ and 3: we use red and green colors for the MSD of particles that are faster than others in the layer. We find a similar behavior for Run #2, while for Run #3 the dynamics is homogeneous within each layer.

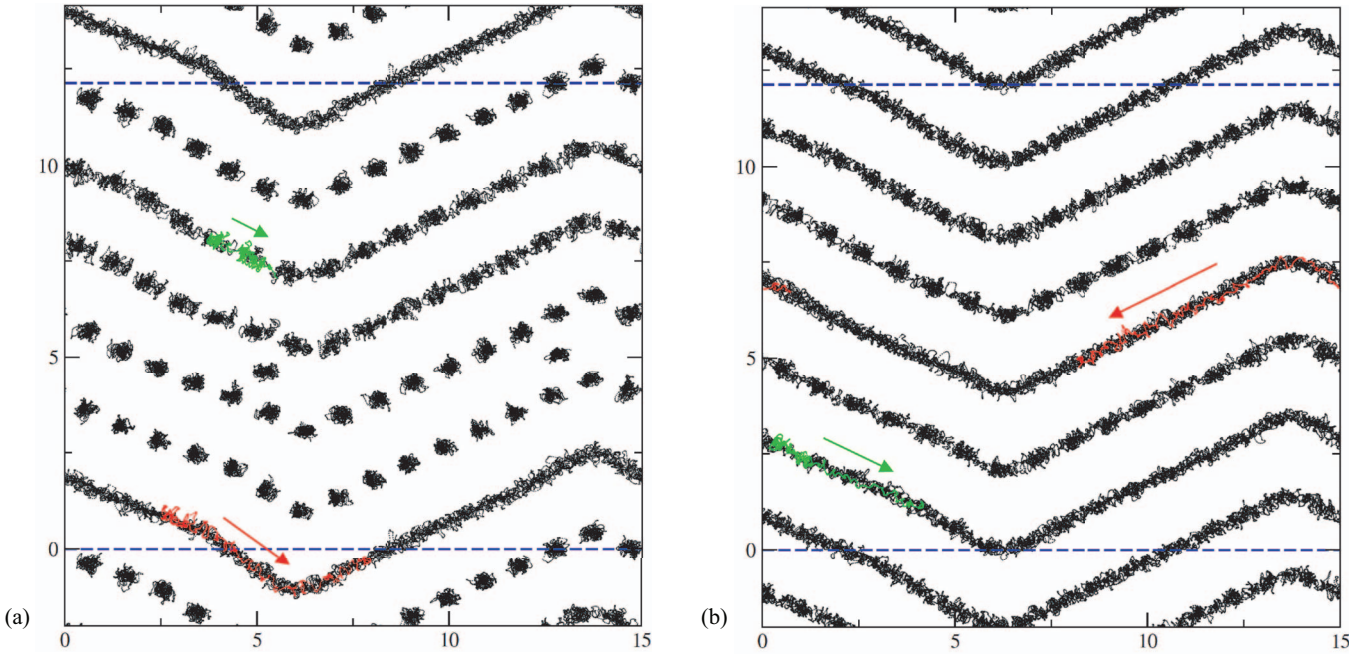

FIG. 12. In-layer trajectories for particles in (a) the second and (b) the third layer of Run #1 in Fig. 10. In red and green, we show the trajectories of representative particles belonging to stripes veins. The MSD of these particles is represented with the same color code as in Fig. 11. We apply periodic boundary conditions along x and y axes at $x = 0$, $x = 15$ and at $y = 0$, $y = 12.1$ (dashed lines). We observe two point-like defects between the stripes near the veins in (a).

and if the veins are related to point-like defects as seems to be suggested by Fig. 12.

IV. DISCUSSION AND CONCLUSIONS

By studying structural and dynamical properties with MD simulations of an anomalous fluid—CSW particles[68–70]—confined between an attractive and structured wall and a repulsive and unstructured wall in a slit pore configuration, we show that the effect of the structured attractive wall can extend up to the entire slit pore. We observe that the particles organize in an inhomogeneous way, forming layers that are parallel to the surfaces, with higher density near the attractive surface with respect to the center of the slit pore. For sufficiently high densities, for which the fluid occupy entirely the pore, we observe an increase of density also close to the repulsive surface, but in a less prominent way, consistent with experimental and theoretical works for nanoconfined fluids.

At low temperature, we find coexistence between the homogeneous liquid, heterogeneous liquid and solid, organized in different layers. The homogeneous liquid corresponds to layers characterized by a flat density profile (apart from fluctuations), an in-layer radial distribution function without structures, an in-layer MSD with diffusive regime and an in-layer SP with the same characteristic decay time $\tau_{\max}$ for each layer. The heterogeneous liquid differs from the homogeneous fluid for a structured, non-flat, density profile and an in-layer SP with different characteristic decay time $\tau_{\max}$ for each layer that composes it. Finally, the solid phase has an in-layer radial distribution function with structures and a homogeneous, arrested dynamics, as shown by the in-layer MSD and SP.

At low T and high ρ, we find a strong structural correlation between the attractive surface and the first layer suggesting a "templating" effect. Indeed, the large density of attractive surface induces the formation of a first layer at high density. The high energy cost of this first layer is compensated by the large number of attractive interactions between the particles of the first layer and those of the surface.

Moving further from the wall, we find that the first layer has a "molding" effect on the second layer. This is because the density of the first layer is smaller than that of the surface and is not high-enough to propagate its template. Nevertheless, the low-density second layer is in condition to template the third layer replicating its structure and inducing a long-range effect that can, eventually, involve the whole system.

From the calculation of the MSD and the Voronoi tessellation we conclude that at low temperature the first layer close to the attractive surface is a polycrystal with two competing phases that generate low-energy states with high degeneracy and very slow dynamics. At low densities the two competing phases are stripes and hexagonal lattice, while at high densities are triangular and Kagome lattice. We understand this result as a consequence of the high density (triangular) structure of the attractive wall with a lattice step that corresponds to the hard repulsive distance of the liquid, and the strong wall-liquid attractive interaction.

These properties of the wall generate in the first liquid layer local regions with density and energy that are higher than the average of the layer. As a consequence, other regions within the layer have density and energy below the average, giving rise to a competing crystal structure.

Our results remind us of some recent experiments and simulations for a thin-film of water on $BaF_2(111)$ surface for which the authors found a very-high-density first interfacial layer for all temperatures, while they would expect, from thermodynamic arguments, a lower density liquid at supercooled conditions.[41] In other recent experiments and

simulations,[44,45] the authors pointed out that it is necessary to revise the theory of heterogeneous nucleation when the crystallization induces a non-zero entropy at zero temperature and the system initially is far from equilibrium.

Apart from the layers close to the two surfaces, we observe that the structure of each layer mainly depends on its density. In the case of the stripe phase, using simple geometrical and energetic considerations, we find that straight and zigzagging stripes are the stable configurations for intermediate densities.

Furthermore, analysing the MSD layer by layer, we find two kinds of heterogeneity in the dynamics. First, we observe that the dynamics is largely heterogeneous among the layers, as a consequence of the sequence of structures caused by the walls presence.

Second, we find layers at high densities and low temperatures with a caging-like behavior characterized by a ballistic dynamics followed by an arrested state (plateau) and a superdiffusive regime with a diffusion exponent $1 < \alpha < 2$. Our analysis shows that this behavior is due to dynamics heterogeneity within the layer as a consequence of the formation of liquid veins in the stripe phase. In particular, we observe that each vein can behave differently from the others, diffusing in one of the two possible directions along the stripes and having a different diffusion exponent $1 < \alpha < 2$.

We rationalize the different possible values of α as a consequence of the presence of residual stress that could introduce an effective force acting on the fluid. Under suitable conditions, e.g., a constant effective force along the stripe, the particles in the vein could perform a biased one-dimensional random walk characterized by an exponent of the MSD that approaches the ballistic value ($\alpha = 2$).

The behavior of these veins can be analyzed in a more quantitative way by computing, for example, the temporal autocorrelation function, the intermediate scattering function,[85,86] the relative displacement of nearest neighbors, or the particles displacements following the Lindemann criterion.[87] We plan to present this analysis in future works.

Our results about the heterogeneous dynamics near the walls, as a consequence of formation of liquid veins within a frozen matrix of liquid, show that the slowing down of the dynamics of the anomalous liquid near the walls does not imply by necessity the complete freezing of the first layers. Therefore, under these considerations, the partial freezing of the first layer does not correspond necessarily to an effective reduction of the channel section in terms of transport properties, at variance with the conclusions of other authors.[88]

ACKNOWLEDGMENTS

We thank Y. Shokef for useful discussion on stripes formation. We acknowledge the support of Spanish MICINN Grant No. FIS2009-10210 and Spanish MEC Grant No. FIS2012-31025. G.F. acknowledges the EU FP7 Grant No. NMP4-SL-2011-266737.

[1]M.-C. Bellissent-Funel, S. H. Chen, and J.-M. Zanotti, Phys. Rev. E **51**, 4558 (1995).
[2]M. Schoen and D. J. Diestler, J. Chem. Phys. **109**, 5596 (1998).
[3]T. M. Truskett, P. G. Debenedetti, and S. Torquato, J. Chem. Phys. **114**, 2401 (2001).
[4]R. J. Mashl, S. Joseph, N. R. Aluru, and E. Jakobsson, Nano Lett. **3**, 589 (2003).
[5]J. Mittal, T. M. Truskett, J. R. Errington, and G. Hummer, Phys. Rev. Lett. **100**, 145901 (2008).
[6]G. Cicero, J. C. Grossman, E. Schwegler, F. Gygi, and G. Galli, J. Am. Chem. Soc. **130**, 1871 (2008).
[7]A. De Virgiliis, R. L. C. Vink, J. Horbach, and K. Binder, Phys. Rev. E **78**, 041604 (2008).
[8]F. Mallamace, C. Corsaro, M. Broccio, C. Branca, N. González-Segredo, J. Spooren, S. H. Chen, and H. E. Stanley, Proc. Natl. Acad. Sci. U.S.A. **105**, 12725 (2008).
[9]N. Giovambattista, P. J. Rossky, and P. G. Debenedetti, J. Phys. Chem. B **113**, 13723 (2009).
[10]S. R.-V. Castrillón, N. Giovambattista, I. A. Aksay, and P. G. Debenedetti, J. Phys. Chem. B **113**, 7973 (2009).
[11]S. R.-V. Castrillón, N. Giovambattista, I. A. Aksay, and P. G. Debenedetti, J. Phys. Chem. B **113**, 1438 (2009).
[12]R. Mancinelli, S. Imberti, A. K. Soper, K. H. Liu, C. Y. Mou, F. Bruni, and M. A. Ricci, J. Phys. Chem. B **113**, 16169 (2009).
[13]P. Gallo, M. Rovere, and S.-H. Chen, J. Phys.: Condens. Matter **22**, 284102 (2010).
[14]W. Rzysko, A. Patrykiejew, S. Sokolowski, and O. Pizio, J. Chem. Phys. **132**, 164702 (2010).
[15]S. Han, M. Y. Choi, P. Kumar, and H. E. Stanley, Nat. Phys. **6**, 685 (2010).
[16]F. de los Santos and G. Franzese, J. Phys. Chem. B **115**, 14311 (2011).
[17]S. K. Schnell, T. J. H. Vlugt, J.-M. Simon, D. Bedeaux, and S. Kjelstrup, Chem. Phys. Lett. **504**, 199 (2011).
[18]S. K. Schnell, T. J. H. Vlugt, J.-M. Simon, D. Bedeaux, and S. Kjelstrup, Mol. Phys. **110**, 1069 (2012).
[19]R. R. Nair, H. A. Wu, P. N. Jayaram, I. V. Grigorieva, and A. K. Geim, Science **335**, 442 (2012).
[20]D. R. Paul, Science **335**, 413 (2012).
[21]A. L. Ferguson, N. Giovambattista, P. J. Rossky, A. Z. Panagiotopoulos, and P. G. Debenedetti, J. Chem. Phys. **137**, 144501 (2012).
[22]M. C. Stewart and R. Evans, Phys. Rev. E **86**, 031601 (2012).
[23]L. B. Krott and M. C. Barbosa, J. Chem. Phys. **138**, 084505 (2013).
[24]G. Schirò, A. Cupane, E. Vitrano, and F. Bruni, J. Phys. Chem. B **113**, 9606 (2009).
[25]S. Karan, S. Samitsu, X. Peng, K. Kurashima, and I. Ichinose, Science **335**, 444 (2012).
[26]F. Biedermann, M. Vendruscolo, O. A. Scherman, A. De Simone, and W. M. Nau, J. Am. Chem. Soc. **135**, 14879 (2013).
[27]G. Franzese and V. Bianco, Food Biophys. **8**, 153 (2013).
[28]N. Giovambattista, P. Rossky, and P. Debenedetti, Annu. Rev. Phys. Chem. **63**, 179 (2012).
[29]T. Urbic, V. Vlachy, and K. A. Dill, J. Phys. Chem. B **110**, 4963 (2006).
[30]N. Giovambattista, P. J. Rossky, and P. G. Debenedetti, Phys. Rev. E **73**, 041604 (2006).
[31]N. Giovambattista, P. J. Rossky, and P. G. Debenedetti, Phys. Rev. Lett. **102**, 050603 (2009).
[32]K. B. Jinesh and J. W. M. Frenken, Phys. Rev. Lett. **101**, 036101 (2008).
[33]K. Koga, X. C. Zeng, and H. Tanaka, Phys. Rev. Lett. **79**, 5262 (1997).
[34]J. Slovák, K. Koga, H. Tanaka, and X. C. Zeng, Phys. Rev. E **60**, 5833 (1999).
[35]R. Zangi and A. E. Mark, Phys. Rev. Lett. **91**, 025502 (2003).
[36]V. W. A. de Villeneuve, R. P. A. Dullens, D. G. A. L. Aarts, E. Groeneveld, J. H. Scherff, W. K. Kegel, and H. N. W. Lekkerkerker, Science **309**, 1231 (2005).
[37]D. T. Limmer and D. Chandler, J. Chem. Phys. **137**, 044509 (2012).
[38]J. R. Bordin, L. B. Krott, and M. C. Barbosa, J. Phys. Chem. C **118**, 9497 (2014).
[39]Y. Liu, A. Z. Panagiotopoulos, and P. G. Debenedetti, J. Chem. Phys. **132**, 144107 (2010).
[40]V. Bianco and G. Franzese, Sci. Rep. **4**, 4440 (2014).
[41]S. Kaya, D. Schlesinger, S. Yamamoto, J. T. Newberg, H. Bluhm, H. Ogasawara, T. Kendelewicz, G. E. Brown, L. G. M. Pettersson, and A. Nilsson, Sci. Rep. **3**, 1074 (2013).
[42]M. C. Foster and G. E. Ewing, J. Chem. Phys. **112**, 6817 (2000).
[43]V. Sadtchenko, P. Conrad, and G. E. Ewing, J. Chem. Phys. **116**, 4293 (2002).
[44]S. J. Cox, S. M. Kathmann, J. A. Purton, M. J. Gillan, and A. Michaelides, Phys. Chem. Chem. Phys. **14**, 7944 (2012).

[45]Q. Chen, S. C. Bae, and S. Granick, Nature (London) **469**, 381 (2011).
[46]G. Malescio and G. Pellicane, Nat. Mater. **2**, 97 (2003).
[47]M. A. Glaser, G. M. Grason, R. D. Kamien, A. Košmrlj, C. D. Santangelo, and P. Ziherl, EPL **78**, 46004 (2007).
[48]Y. von Hansen, S. Gekle, and R. R. Netz, Phys. Rev. Lett. **111**, 118103 (2013).
[49]Y. Zhang, A. Faraone, W. A. Kamitakahara, K.-H. Liu, C.-Y. Mou, J. B. Leão, S. Chang, and S.-H. Chen, Proc. Natl. Acad. Sci. U.S.A. **108**, 12206 (2011).
[50]A. K. Soper, Proc. Natl. Acad. Sci. U.S.A. **108**, E1192 (2011).
[51]Y. Zhang, A. Faraone, W. A. Kamitakahara, K.-H. Liu, C.-Y. Mou, J. B. Leão, S. Chang, and S.-H. Chen, Proc. Natl. Acad. Sci. U.S.A. **108**, E1193 (2011).
[52]J. Bai and X. C. Zeng, Proc. Natl. Acad. Sci. U.S.A. **109**, 21240 (2012).
[53]J. C. Palmer, F. Martelli, Y. Liu, R. Car, A. Z. Panagiotopoulos, and P. G. Debenedetti, Nature (London) **510**, 385 (2014).
[54]F. Smallenburg, L. Filion, and F. Sciortino, Nat. Phys. **10**, 653 (2014).
[55]E. A. Jagla, Phys. Rev. E **58**, 1478 (1998).
[56]G. Franzese, G. Malescio, A. Skibinsky, S. V. Buldyrev, and H. E. Stanley, Nature (London) **409**, 692 (2001).
[57]G. Franzese, G. Malescio, A. Skibinsky, S. V. Buldyrev, and H. E. Stanley, Phys. Rev. E **66**, 051206 (2002).
[58]A. Skibinsky, S. V. Buldyrev, G. Franzese, G. Malescio, and H. E. Stanley, Phys. Rev. E **69**, 061206 (2004).
[59]G. Malescio, G. Franzese, A. Skibinsky, S. V. Buldyrev, and H. E. Stanley, Phys. Rev. E **71**, 061504 (2005).
[60]Z. Yan, S. V. Buldyrev, N. Giovambattista, and H. E. Stanley, Phys. Rev. Lett. **95**, 130604 (2005).
[61]L. Xu, P. Kumar, S. V. Buldyrev, S.-H. Chen, P. H. Poole, F. Sciortino, and H. E. Stanley, Proc. Natl. Acad. Sci. U.S.A. **102**, 16558 (2005).
[62]A. B. de Oliveira, P. A. Netz, T. Colla, and M. C. Barbosa, J. Chem. Phys. **124**, 084505 (2006).
[63]A. B. de Oliveira, P. A. Netz, T. Colla, and M. C. Barbosa, J. Chem. Phys. **125**, 124503 (2006).
[64]G. Franzese and H. E. Stanley, J. Phys.: Condens. Matter **19**, 205126 (2007).
[65]N. M. Barraz, Jr., E. Salcedo, and M. C. Barbosa, J. Chem. Phys. **131**, 094504 (2009).
[66]B. Guillot, J. Mol. Liq. **101**, 219 (2002).
[67]T. Dotera, T. Oshiro, and P. Ziherl, Nature (London) **506**, 208 (2014).
[68]G. Franzese, J. Mol. Liq. **136**, 267 (2007).
[69]A. B. de Oliveira, G. Franzese, P. A. Netz, and M. C. Barbosa, J. Chem. Phys. **128**, 064901 (2008).
[70]P. Vilaseca and G. Franzese, J. Chem. Phys. **133**, 084507 (2010).
[71]P. Vilaseca, K. A. Dawson, and G. Franzese, Soft Matter **9**, 6978 (2013).
[72]L. D. Gelb, K. E. Gubbins, R. Radhakrishnan, and M. Sliwinska-Bartkowiak, Rep. Prog. Phys. **62**, 1573 (1999).
[73]R. Zangi, J. Phys.: Condens. Matter **16**, S5371 (2004).
[74]P. Bladon and D. Frenkel, Phys. Rev. Lett. **74**, 2519 (1995).
[75]H. Löwen, Physica A **235**, 129 (1997), in Proceedings of the Workshop on Colloid Physics.
[76]A. H. Marcus and S. A. Rice, Phys. Rev. E **55**, 637 (1997).
[77]T. Bryk, S. De Panfilis, F. A. Gorelli, E. Gregoryanz, M. Krisch, G. Ruocco, M. Santoro, T. Scopigno, and A. P. Seitsonen, Phys. Rev. Lett. **111**, 077801 (2013).
[78]P. Vilaseca and G. Franzese, J. Non-Cryst. Solids **357**, 419 (2011), in Proceedings of the 6th International Discussion Meeting on Relaxation in Complex Systems.
[79]M. P. Allen and D. J. Tildesley, *Computer Simulation of Liquids* (Oxford University Press, 1989).
[80]F. Varnik, J. Baschnagel, and K. Binder, J. Chem. Phys. **113**, 4444 (2000).
[81]See supplementary material at http://dx.doi.org/10.1063/1.4899256 for the details about the pressure calculation, the templating effect on the first layer, formation of stripes.
[82]T. G. Lombardo, N. Giovambattista, and P. G. Debenedetti, Faraday Discuss. **141**, 359 (2009).
[83]S. J. Gerbode, U. Agarwal, D. C. Ong, C. M. Liddell, F. Escobedo, and I. Cohen, Phys. Rev. Lett. **105**, 078301 (2010).
[84]D. Banerjee, S. V. Bhat, and D. Leporini, PLoS ONE **7**, e44382 (2012).
[85]A. A. Milischuk, V. Krewald, and B. M. Ladanyi, J. Chem. Phys. **136**, 224704 (2012).
[86]T. S. Ingebrigtsen, J. R. Errington, T. M. Truskett, and J. C. Dyre, Phys. Rev. Lett. **111**, 235901 (2013).
[87]K. Zahn, R. Lenke, and G. Maret, Phys. Rev. Lett. **82**, 2721 (1999).
[88]E. G. Solveyra, E. d. l. Llave, V. Molinero, G. J. A. A. Soler-Illia, and D. A. Scherlis, J. Phys. Chem. C **117**, 3330 (2013).